Langley Gran
IN-02 - CR
140735
24 p.

Progress Report

Pressure Measurements of Impinging Jet with Asymmetric Nozzle

Grant No. NAG-1-819

submitted to

NASA Langley Research Center
Hampton, VA 23665

Attention: J. M. Seiner

by

Department of Aerospace Engineering
University of Southern California
University Park
Los Angeles, California 90089-1191

Principal Investigator:
Ho, Chih-Ming, Professor
(213)743-6560

Date: May 1988

THE NEAR-FIELD PRESSURE FLUCTUATIONS OF AN

IMPINGING ELLIPTIC JET

Principal Investigator: Ho, Chih-Ming, Professor

Department of Aerospace Engineering

University of Southern California

Los Angeles, California 90089-1191

ABSTRACT

For modern aircraft, impinging surfaces are commonly used as a device for obtaining vector thrust from engine exhaust. The nature of dynamic loading is important to understand for design purposes. In this study, we examine the frequency, mode and level of pressure fluctuations generated by an elliptic jet. The elliptic jet is used because it has several operational advantages over a circular jet.

1 INTRODUCTION

When a jet issues from the nozzle, a thin shear layer forms between the high speed stream and the ambient. The shear layer is unstable and develops Kelvin-Helmholtz instability waves. Eventually, the vorticity lumps into large vortical structures.[1] When the structure convects with the free stream flow, it generates pressure fluctuations. Near the jet, the pressure fluctuations are of the hydrodynamic type. The propagation speed and the amplitude of the pressure waves scale with the jet speed. Far away from the jet, the pressure

1

waves propagate at sonic speed and the intensity is proportional to the eighth power of the jet speed. In the past, flow generated acoustic waves have been extensively studied for the purpose of better environmental protection.[2,3,4,5] On the contrary, the hydrodynamic pressure field is not fully explored.[6] Recently, due to the applications of composite materials and the use of vectored thrust devices, an accurate pressure loading has become necessary for proper design of the loading surface.

Most conventional jets have a circular exhaust. The instability waves and coherent structures can develop in axisymmetric or higher modes.[7,8,9] The near-field pressure fluctuations induced by these structures also exhibit a combination of many modes, but the axisymmetric is the strongest. Recently, it has been found that the jet with an elliptic nozzle can entrain surrounding fluid much more effectively than the circular nozzle.[10] The main mechanism of the large entrainment is the axis switching of the elliptic vortex ring caused by the self-induction. Obviously, the near-field pressure fluctuations will be greatly influenced by the axis switching process. Asymmetric nozzle becomes a common configuration in some modern airplanes. An understanding of the pressure loading is in demand.

When a plate is placed near the jet, the development of the coherent structures will be modified by the feedback of the pressure generated by the impinging vortices. In the case of an elliptic jet, one extra factor is the ratio between the axis switching distance and the nozzle to plate distance because this ratio determines the phase of feedback pressure waves in the plane normal to jet axis. The formation of the vortices will be determined

by the feedback forcing and the dynamic loading is then modified. Therefore, the location and the orientation of the plate is a major parameter in studying the near-field loading problem.

In this project, we studied the pressure fluctuations of both a free and an imping-ing elliptic jet. The levels of loading, the spectral information and the azimuthal phase distribution are examined.

2 FACILITY AND INSTRUMENTATION

Measurements were performed in a small-aspect-ratio elliptic jet located inside the USC anechoic chamber, which has a working dimension of $7.4 \times 4.8 \times 3.6$ m and a low frequency cut-off of 150 Hz. The major diameter of the nozzle $2a$ was 50.8 mm and the minor diameter $2b$ was 25.4 mm. The settling chamber of the nozzle assembly (Fig. 1a) had an inside diameter of 0.38 m. The total contraction ratio was 112:1. Jet flow was driven by a blow-down system and was maintained at a speed of 21.9 m/sec or $Re_{2a} = 7.8 \times 10^4$ in the present experiment. Together with the low noise control valve downstream from the high-pressure storage vessel and silk-screens in the settling chamber, the 5th order polynomial nozzle contour provided an initially laminar boundary layer and a low turbulence level such that the dominating fundamental instability of the jet satisfied linear theory and had a frequency proportional to $U_j^{\frac{1}{2}}$.

Eight Panasonic WM-063X electret microphones were selected for the near-field mea-surements. The dynamic response of the microphones, which had a physical dimension

of 6 mm and were equiped with a home-made power-supply/amplifier, were calibrated locally and shown to have a linear response up to 5 kHz. The impinging plate was mounted vertically at a distance 8a from the jet exit.

Measurements were digitized on line with a PDP11/23 microcomputer. Data reduction was performed with this microcomputer or with a larger VAX/750 computer.

3   EXPERIMENTAL RESULTS

3.1   Loading Level:

We placed eight pressure transducers around the jet, at an equal distance from the axis (Fig. 1b) to measure the fluctuating pressure. At the nozzle, they are located at the jet edge of the major axis side. When they are placed at downstream positions, each transducer is moved along a ray at 12° with respect to the axis. The near-pressure level drops from the jet edge exponentially and then changes to algebraic decay. The exponentially decaying region extends about one hydrodynamic instability wavelength from the jet.[11] The surveyed region of these transducers is within the hydrodynamic near field.

The streamwise fluctuating pressures are shown in Fig. 2. The level of fluctuations increases with distance as the instability wave amplifies. Further downstream, the intensity drops. The measurements near the major axis have higher readings than other positions because the transducers are placed closer to the jet edge. The interesting point is that the level of fluctuations for the impinging case are in general lower than those for the

free jet case. The difference is about as much as 50% before the peak of the distribution. This result indicates that the near field pressure can be altered dramatically by the presence of a nearby structure. It is a significant finding and can be an important factor for design considerations. We will examine the effects of orientation of the impingement and other parameters in more detail. Identifying the physical mechanism of this change is probably the major task for the near future. We speculate that the feedback generated by the impinging vortices delays the development of the vortices in the shear layer. The exact process remains to be clarified. The azimuthal distributions of the free jet and the impinging cases are shown in Fig.3. The lower fluctuation level for the impinging jet is observed around the jet.

The flip-flop between the major and the minor axis is caused by the self-induction of the asymmetric vortex rings. The near field pressure reflects the axis switching phenomenon. At $x/a = 0.48$, the azimuthal profile shows high levels of disturbances near the major axis area because the sensors are closer to the jet (Fig. 4). A $x/a = 5.76$, the switching becomes apparent and the azimuthal distribution of the pressure is opposite, in phase, to the one near the nozzle.

3.2   Spectral and Phase Information

The spectrum taken at the major axis near the nozzle ($x/a = 0.48$, Fig. 5) shows peaks of the fundamental ($\sim$2 kHz), the first subharmonic ($\sim$1 k Hz) and a strong beat at frequency about 1.5 kHz. The pressure spectrum at the minor axis has a different form; the second

5

subharmonic is dominating and the fundamental is not observable. We have found that the extents of the fundamental and the subharmonics are scaled with their own wavelength.[11] The transducer placed near the minor axis is more than one fundamental wavelength away from the jet and therefore the pressure fluctuations at the fundamental frequency are not strong. The dashed lines are the spectra for the impinging jet. The spectra of the free jet have almost the identical shape of the impinging case, but the spectral density is uniformly higher.

At a downstream station ($x/a = 0.85$), the transducers are at about four initial instability wavelengths from the nozzle. This is the location where the first vortex merging takes place (Ho and Gutmark[10]). Near the major axis, the spectra of both free jet and impinging jet are dominated by the peak at the first subharmonic (Fig. 6). The peak at the second subharmonic dominates the spectra near the minor axis.

The elliptic vortex ring not only switches the major and minor axes while it convects with the free stream velocity, but also bends from the plane normal to the jet axis. The phase correlations of the transducers placed in the same plane can reveal the deformation. For example, the two transducers placed at two sides across the major axis have their phase spectrum shown in Fig. 7. The phase differences at all frequencies are close to zero because the rings distort in the same fashion across the jet. The phase spectrum between the two transducers placed at the major and the minor axes have very different forms. The phase difference between the first and the second subharmonics is very large due to the azimuthal deformation of the elliptic vortical structures.

3.3 Pseudo-visualization of the Elliptic Vortices

To construct a display to *visualize* the passage of the vortical structures of an elliptic jet, pressure measurements were acquired from eight microphones mounted on a rack such that the measuring points were evenly distributed azimuthally at a fixed radial location at a plane downstream and parallel to the exit plane. At a certain time t_0, their pressure fluctuations p were plotted versus azimuthal angle ϕ and connected by means of a straight forward interpolation scheme. The measurement at the first azimuthal location was repeated as the ninth measurement in the interpolation because of the circular geometry of the microphone array. Qualitatively, this curve represented the global instantaneous pressure fluctuations at the measuring plane. When the same types of curves were constructed at $t > t_0$ with constant time increments, the resulting imprint showed the passage of the hydrodynamic waves at this imaginary plane. Since the microphones were submerged in the expontentially decaying region of the jet, these imprints also represented the passage of the vortical structures in the jet.

Since microphones would sense waves generated in a fixed neighborhood around themselves, these signals were contaminated and had to be filtered before the pseudo-display scheme could be applied. To avoid phase distortion, a FIR (finite impulse response) digital bandpass filter was applied to the microphone signals. Results were plotted in Figs. 8 to 13. The solid lines were arbitrarily designated for positive pressure fluctuations while the dashed lines were used when fluctuations were negative. For Fig. 8 to 11, the center frequency of the bandpass filter was set at the first subharmonic f_1 such that the distortion

of these structures during the pairing process could be *visualized*. The azimuthal distortion of the imprint at $x/a = 0.85$, Fig. 9, symbolized the deformation of the vortical structures during the pairing process. However, by comparing the imprints of Figs. 10 and 11 to Fig. 9, it was shown that the same types of distortion, hence, the pairing process, were actually delayed by the presence of the impinging plate.

The slight distortion of the structures in Fig. 8 demonstrated the phase deformation caused by the mismatch between the circular microphone-array and the elliptic sound generating region of the jet. Figs. 12 and 13 show the imprints of the vortical structures near the first axis switch location ($x/a \sim 5$).[10] At this location, the cross section of the jet flow turned quite circular and the distortion of the structures in these imprints, unlike the case in Fig. 8, became azimuthally independent. As a matter of fact, the presence of the impinging plate produced more organized vortical structures at this location. However, a quantitative verification of this observation is required.

4   CONCLUSIONS

The important finding in this preliminary study is that the near-field pressure fluctuations for an impinging jet are much lower than those of a free jet. The exact physical mechanism is still under investigation but the importance of this finding to the design of an asymmetric jet nozzle with a nearby structure is obvious.

The near-field pressure fluctuation is a strong function of the location away from the jet because their level decays exponentially with distance and the length scale is the hydrody-

namic instability wavelength. The instability wavelength is about one order of magnitude shorter than the acoustic wavelength in the low Mach number range. Therefore, the spatial structures of near-field pressure are much more convoluted than the acoustic field. The elliptic vortex ring undergoes deformations in and out of the plane normal to the jet axis. The near-field pressure fluctuations are influenced by these distortions. The spatial structure of the fluctuating pressure is further complicated by the deformations.

References

[1] C. M. Ho and P. Huerre, Annual Review of Fluid Mechanics **16**, 365 (1984).

[2] J. E. Ffowcs Williams, **255**, 469 (1963).

[3] D. G. Crighton, Progress in Aerospace Science **16**, 31 (1975).

[4] D. G. Crighton, Journal of Fluid Mechanics **106**, 261 (1981).

[5] M. E. Goldstein, Annual Review of Fluid Mechanics **16**, 263 (1984).

[6] B. Lafouasse, A. Chan, and C. M. Ho, Near field pressure fluctuations of a circular jet, in Aero- and Hydro-Acoustic, pages 403, Springer, Berlin Heidelberg, (1986).

[7] J. Cohen and I. Wygnanski, Journal of Fluid Mechanics **176**, 191 (1987).

[8] J. Cohen and I. Wygnanski, Journal of Fluid Mechanics **176**, 221 235 (1987).

[9] J. K. Wat and R. E. Kaplan, AIAA-86-1911 (1986).

[10] C. M. Ho and E. Gutmark, Journal of Fluid Mechanics **179**, 383 (1987).

[11] C. M. Ho and B. Lafouasse, AIAA-84-2316 (1984).

(a)

(b)
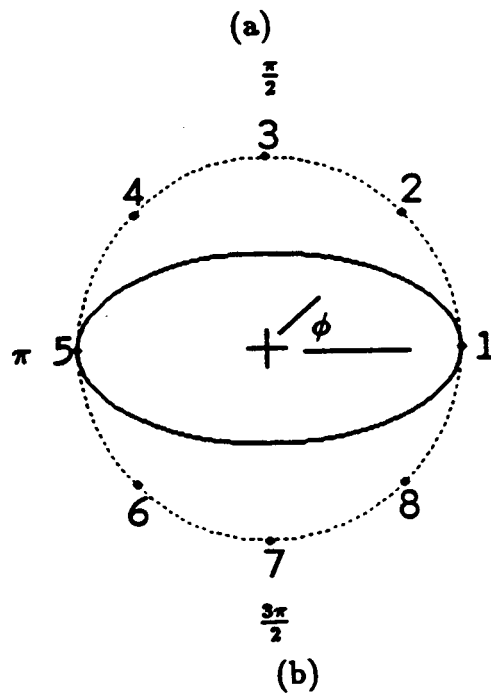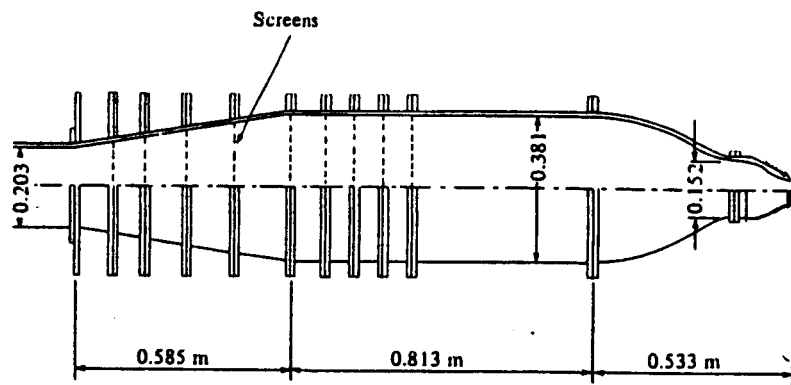
Figure 1: (a) The settling chamber and nozzle assembly and (b) the relative positions between microphones and nozzle outlet.
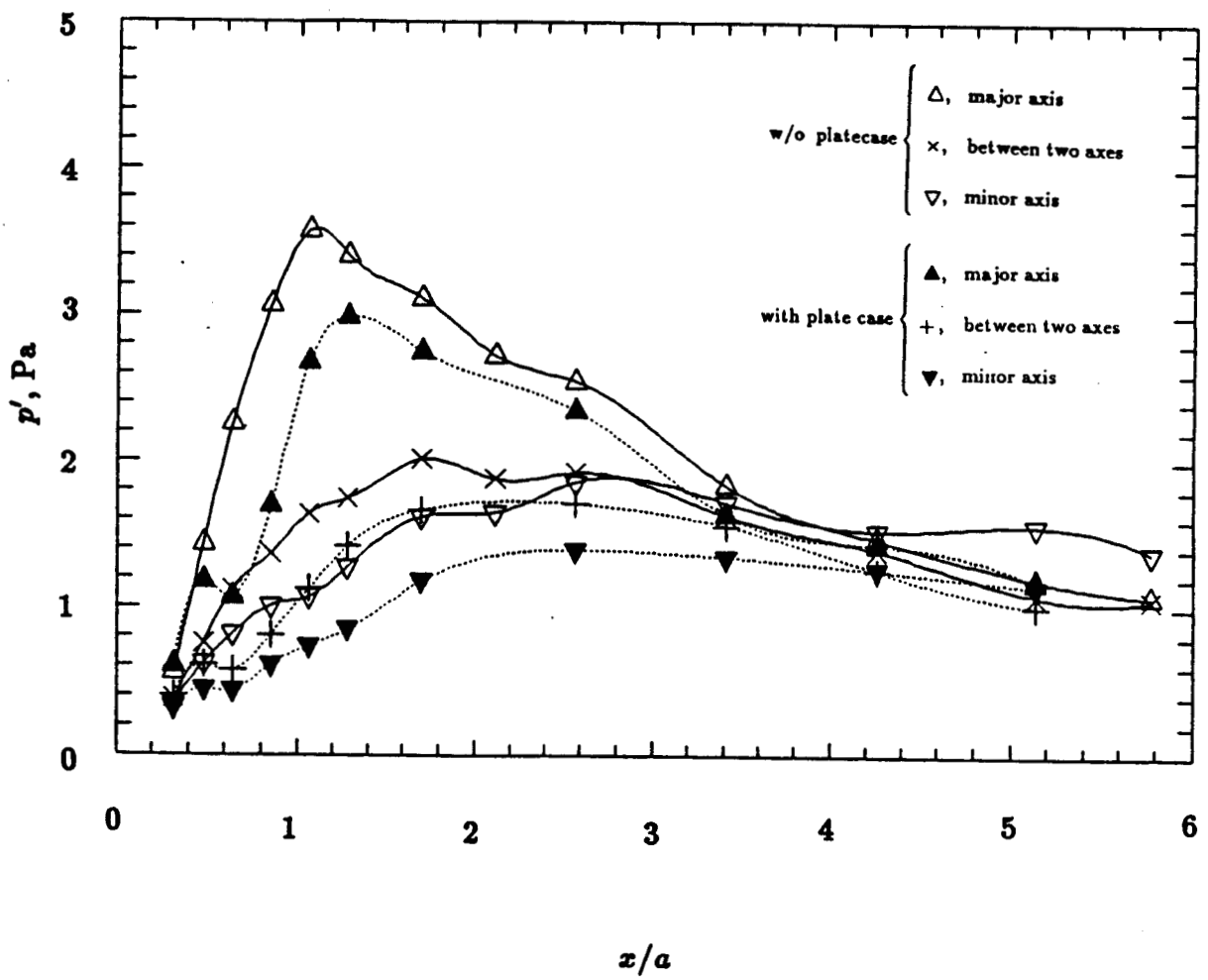
Figure 2: Axial distributions of the average over-all pressure amplitude.
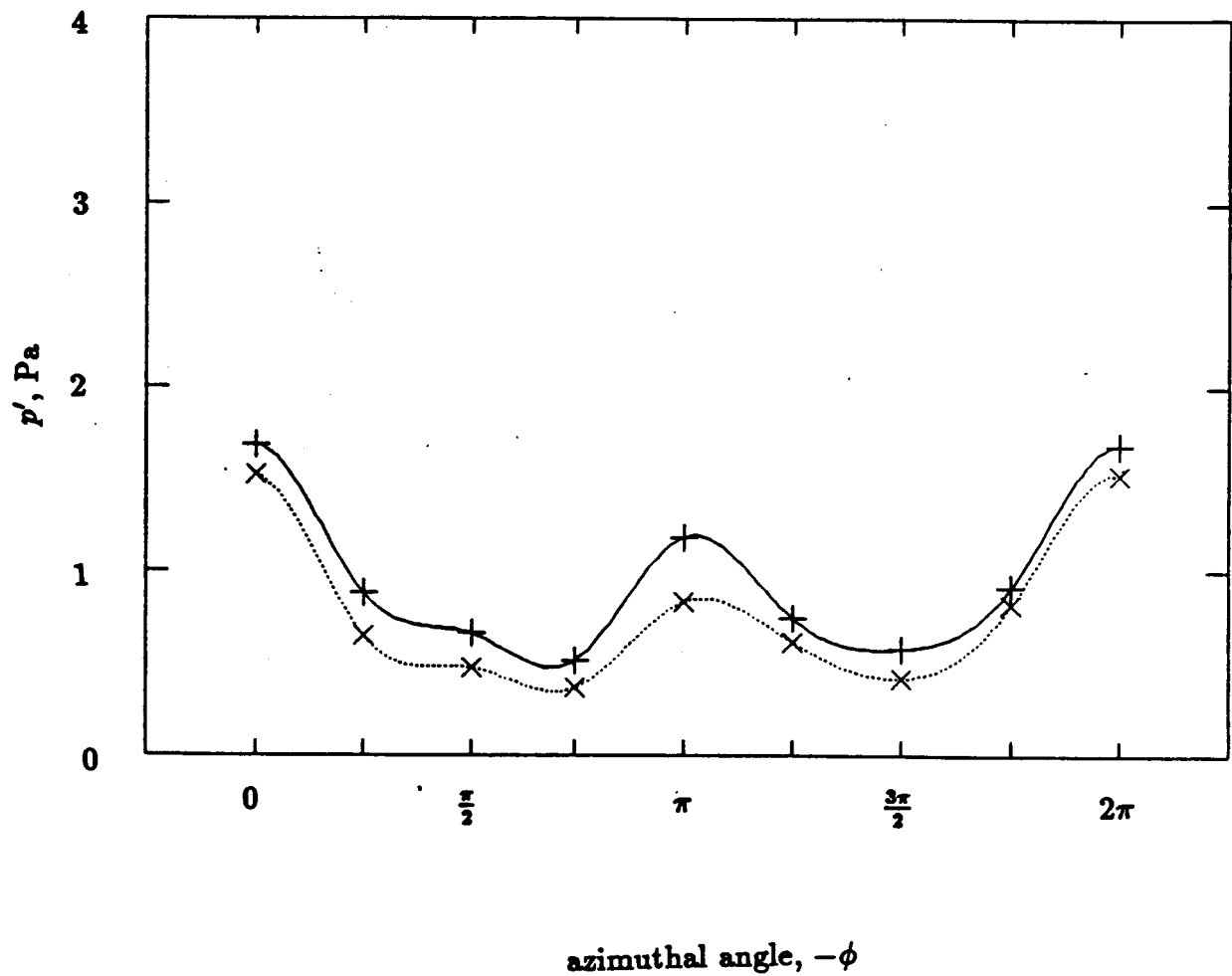
Figure 3: Azimuthal distributions of the over-all pressure amplitude at $x/a = 1.28$: +, without impinging plate and ×, with impinging plate.
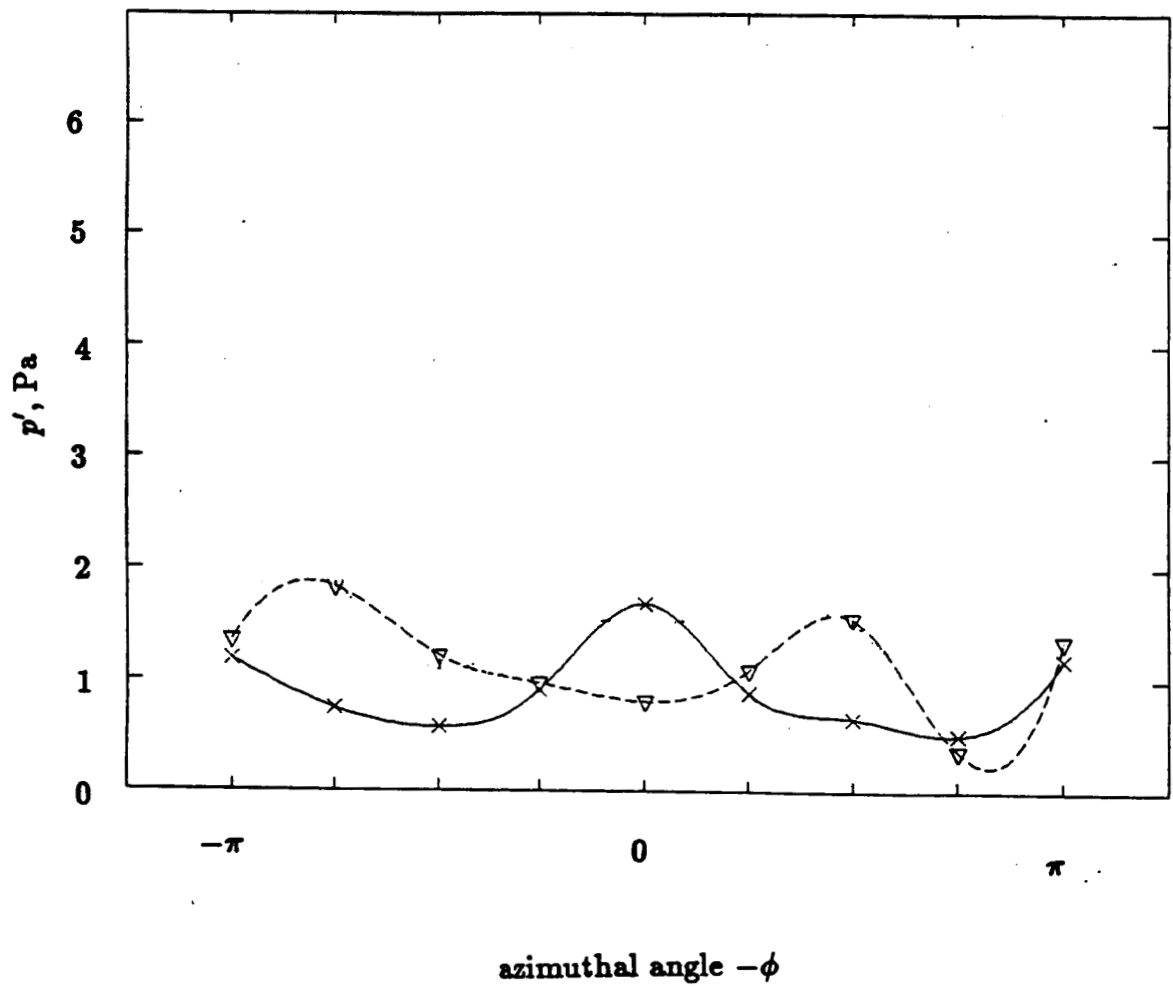
Figure 4: Azimuthal distributions of the over-all pressure amplitude: $\times$, $x/a = 1.28$ and ∇, $x/a = 5.76$. Measurements were performed without the impinging plate installed.
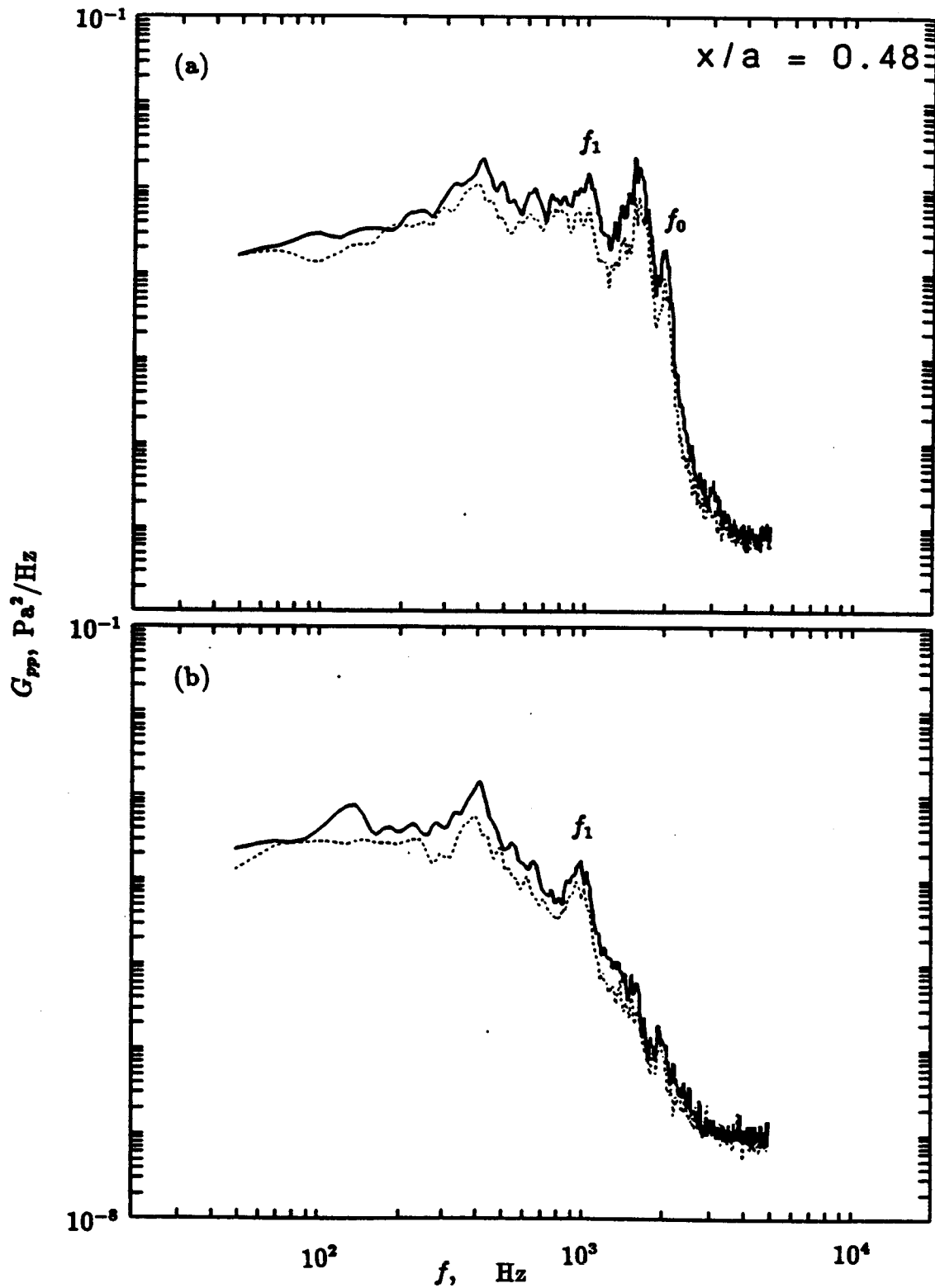
Figure 5: Near-field pressure spectra at $x/a = 0.48$. Microphones were located at $\phi =$ (a) π and (b) $\frac{\pi}{2}$: ——— , without plate case and $\cdots$, with plate case.
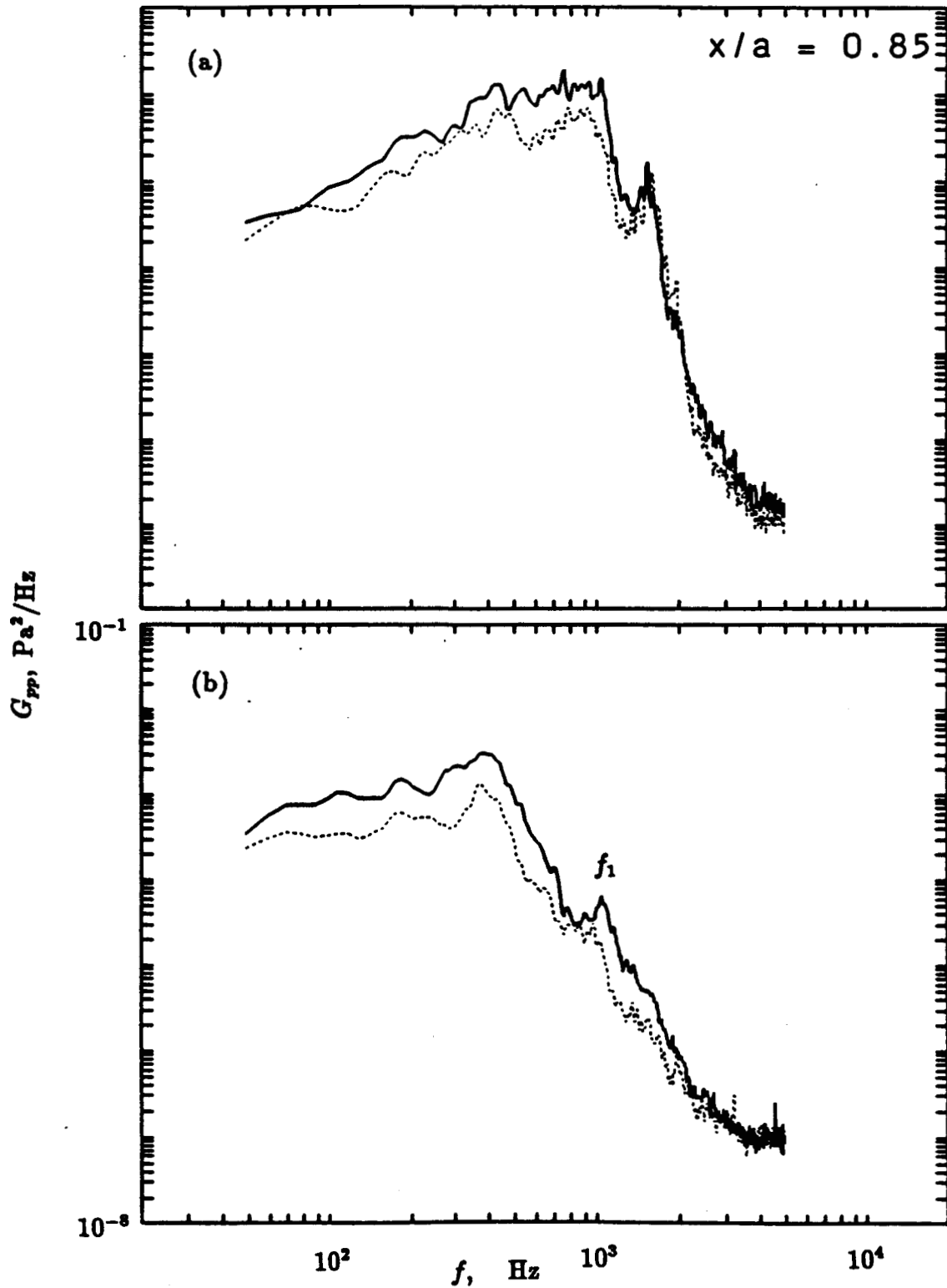
Figure 6: Near-field pressure spectra at $x/a = 0.85$. Microphones were located at $\phi = $ (a) π and (b) $\frac{\pi}{2}$: ———, without plate case and $\cdots$, with plate case.

16
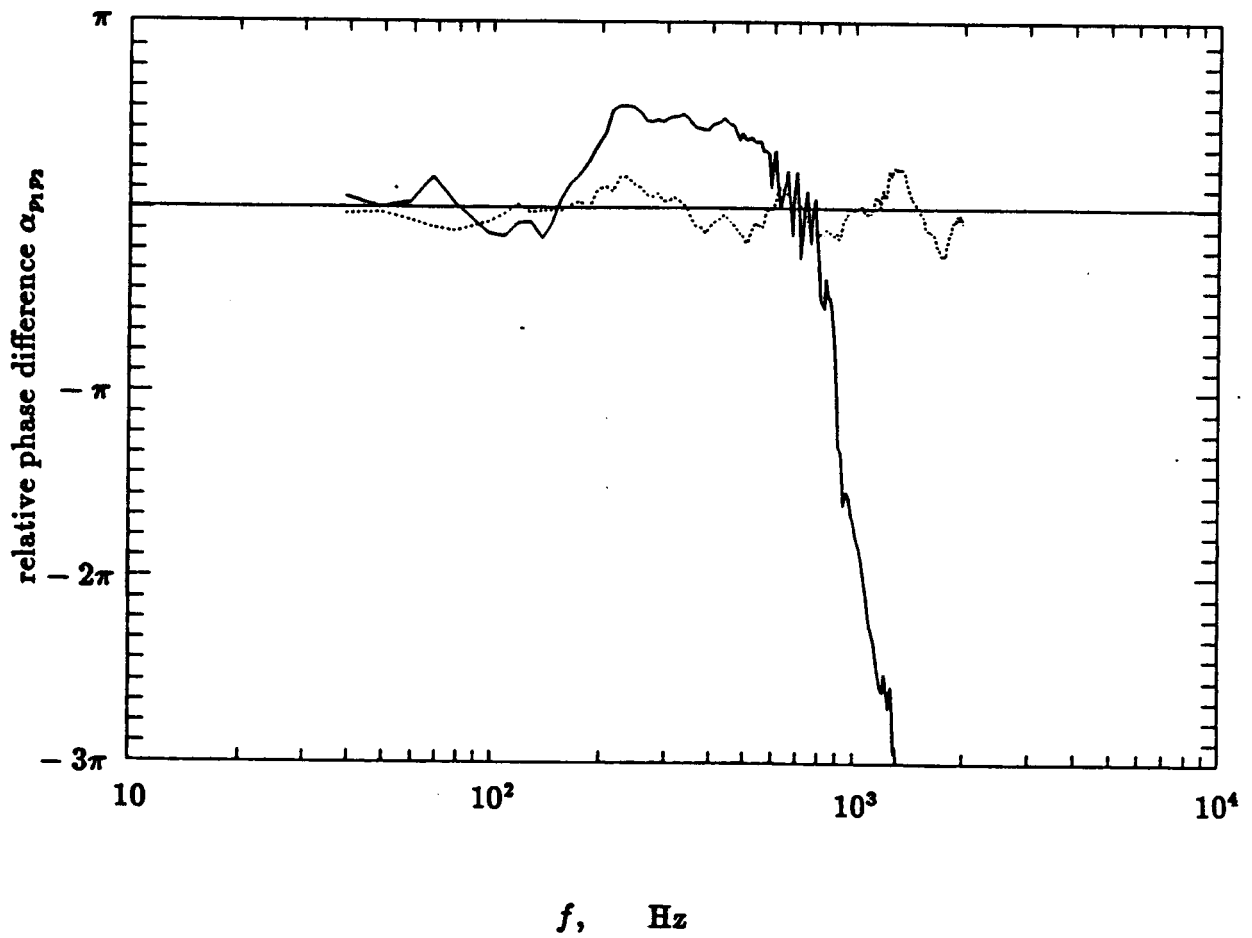
Figure 7: Relative phase difference of the pressure fluctuations measured between $\phi = 0$ and π (——) and between $\phi = \frac{\pi}{2}$ and π ($\cdots$).
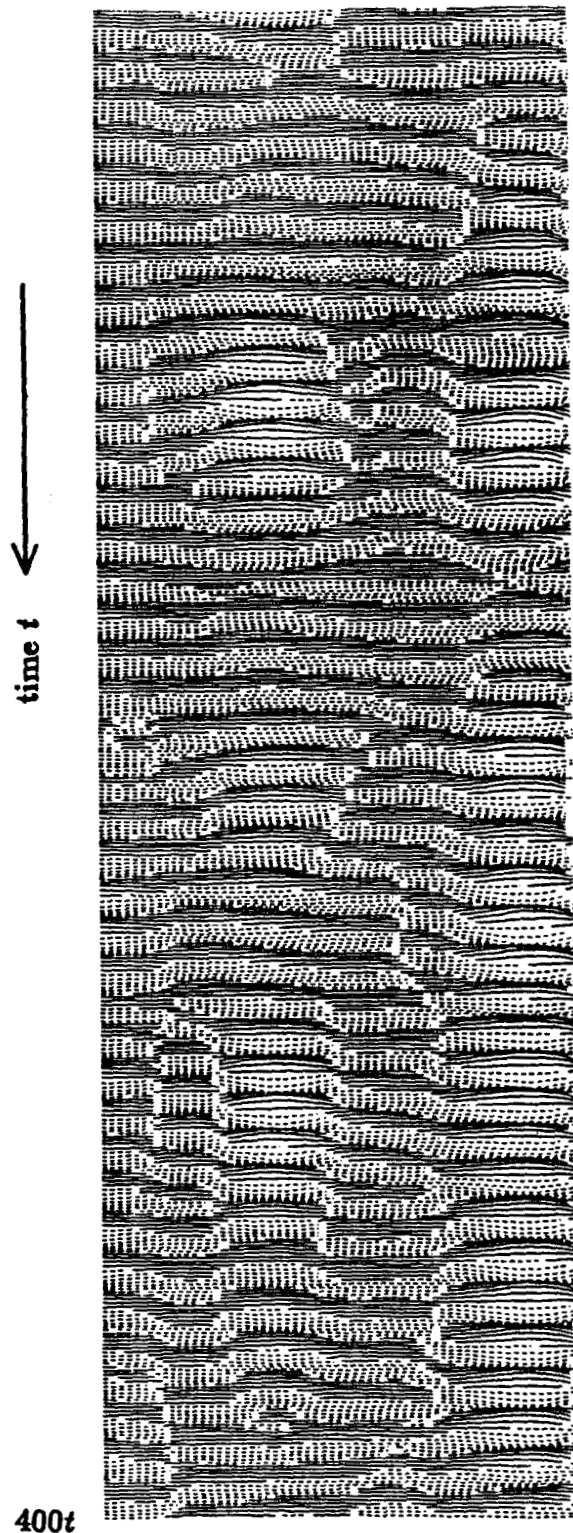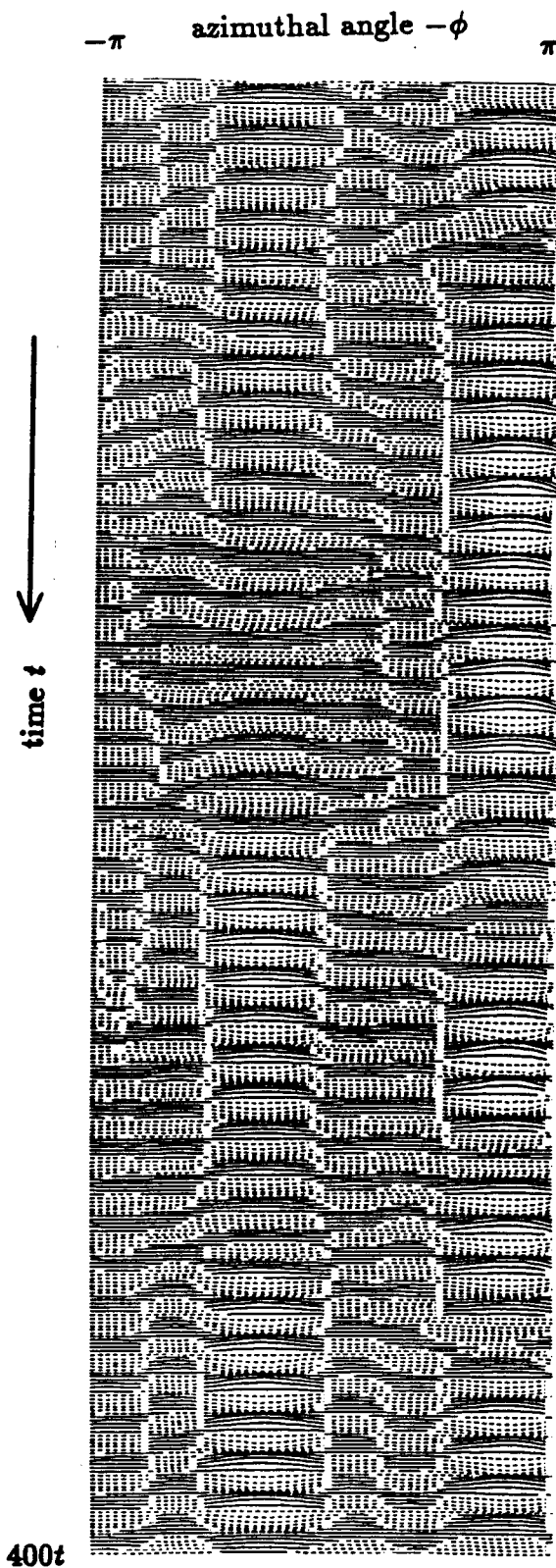
azimuthal angle $-\phi$

$-\pi$ π

time t

$400t$
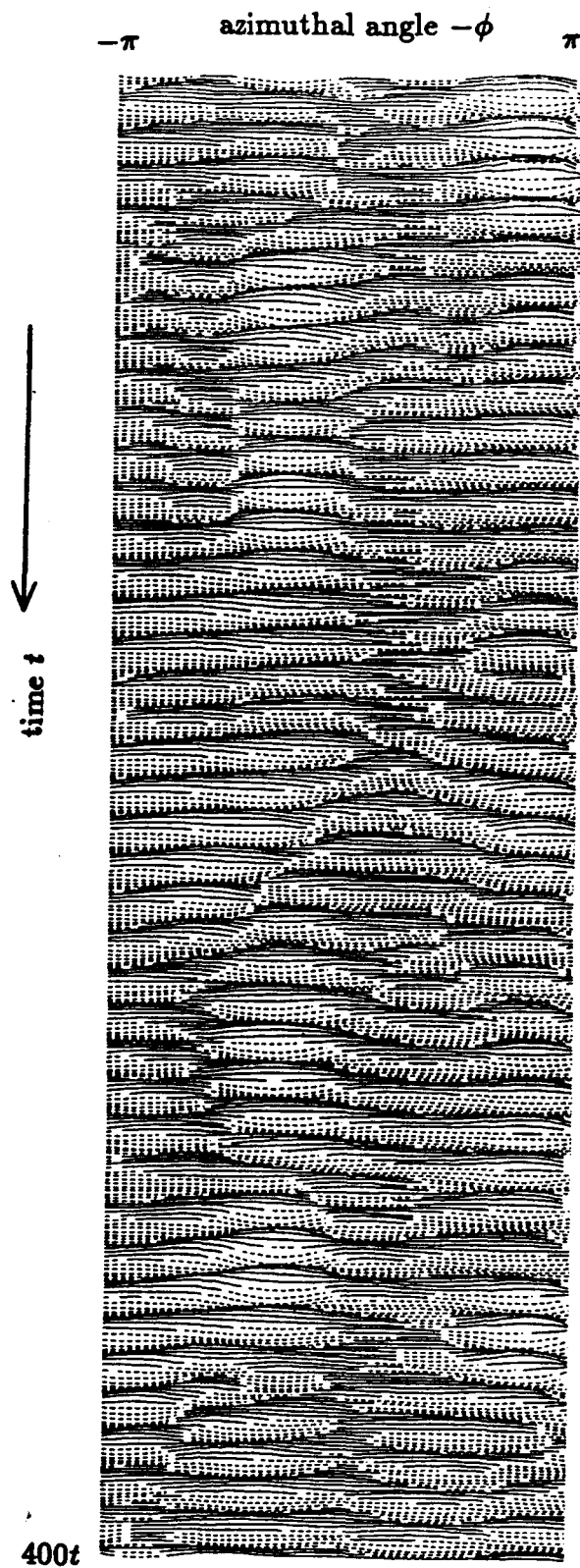
Figure 8: Azimuthal imprints of the vortical structures at $x/a = 0.32$. Signals were bandpass filtered with a $\frac{1}{3}$-octave FIR filter with $f_c = f_1$.

18

azimuthal angle $-\phi$

$-\pi$ $\qquad$ π

time t

$400t$
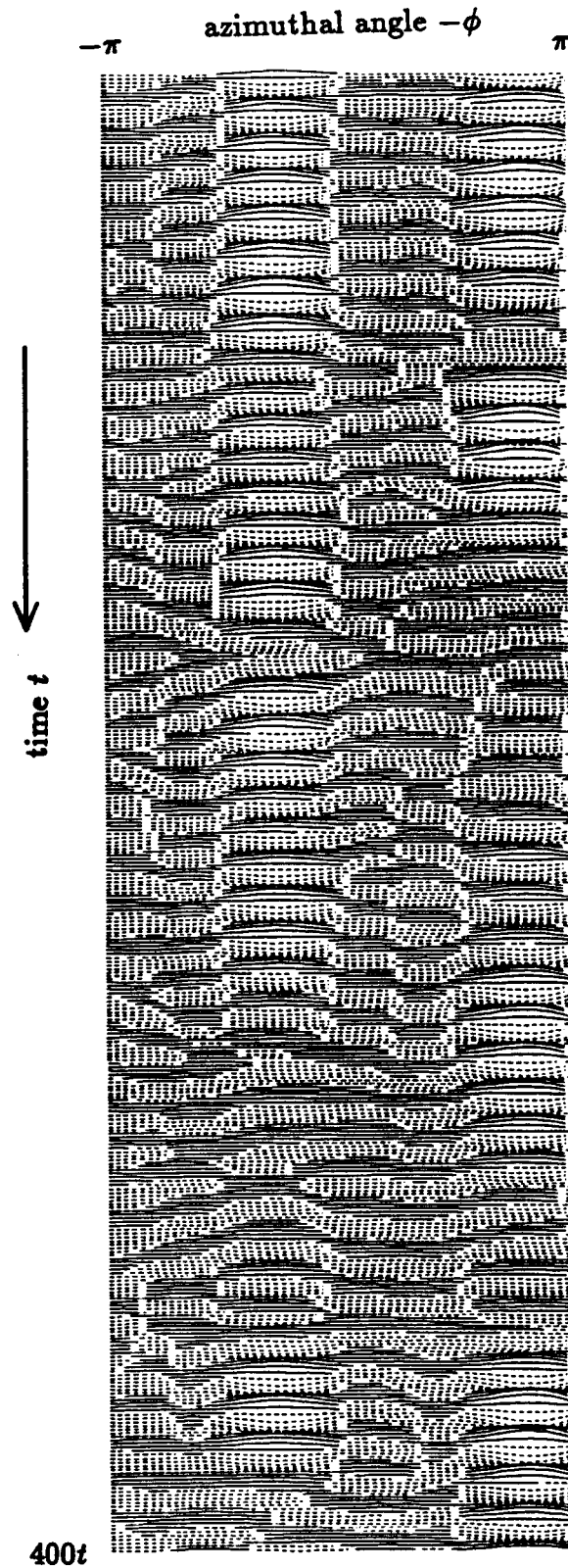
Figure 9: Azimuthal imprints of the vortical structures at $x/a = 0.85$. Signals were bandpass filtered with a $\frac{1}{3}$-octave FIR filter with $f_c = f_1$.
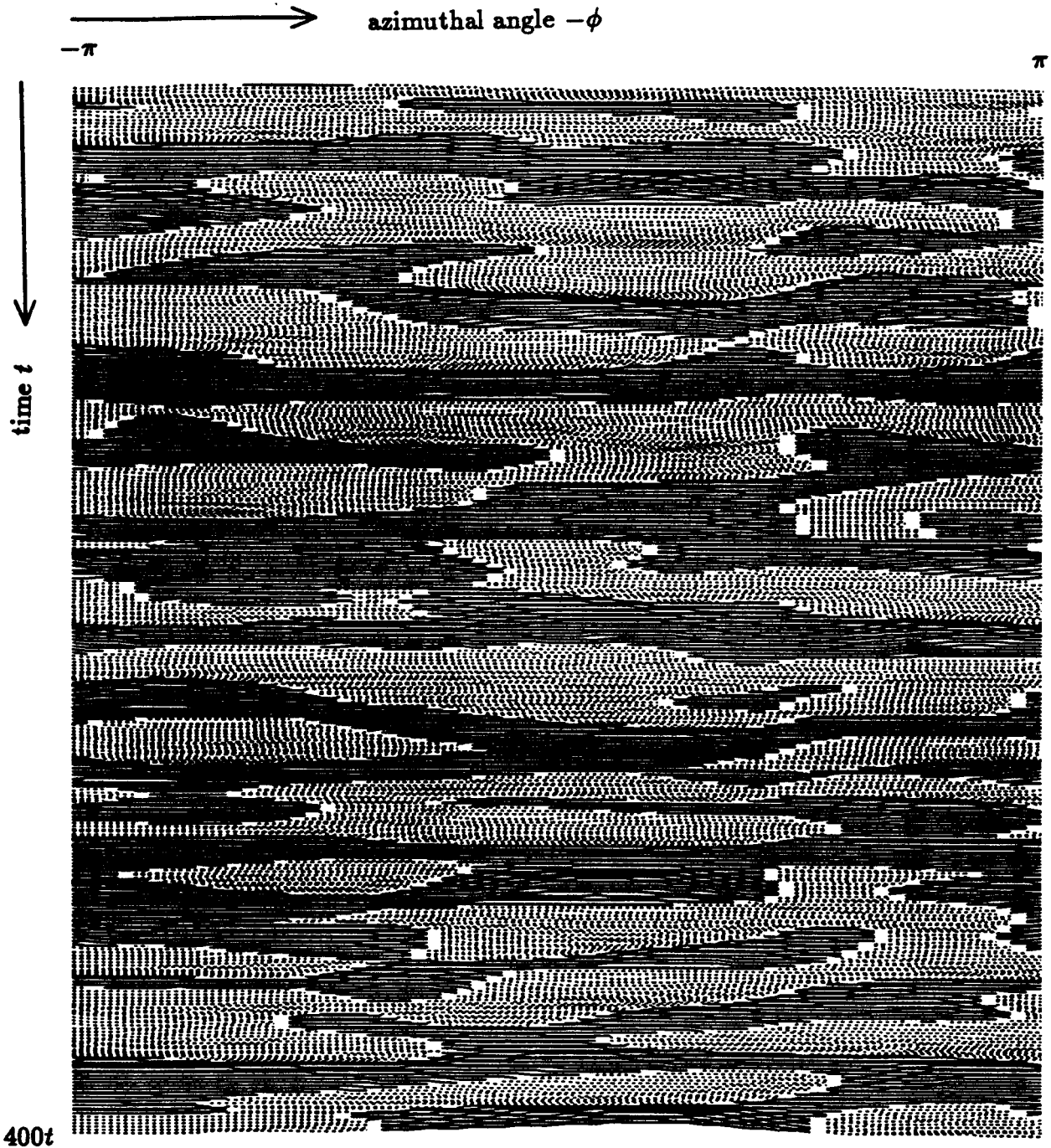
Figure 10: Azimuthal imprints of the vortical structures at $x/a = 0.85$. Signals were bandpass filtered with a $\frac{1}{3}$-octave FIR filter with $f_c = f_1$. Impinging plate was installed in this case.

Figure 11: Azimuthal imprints of the vortical structures at $x/a = 1.06$. Signals were bandpass filtered with a $\frac{1}{3}$-octave FIR filter with $f_c = f_1$. Impinging plate was installed.

Figure 12: Azimuthal imprints of the vortical structures at $x/a = 5.76$. Signals were bandpass filtered with a $\frac{1}{3}$-octave FIR filter with $f_c = 70$ Hz.
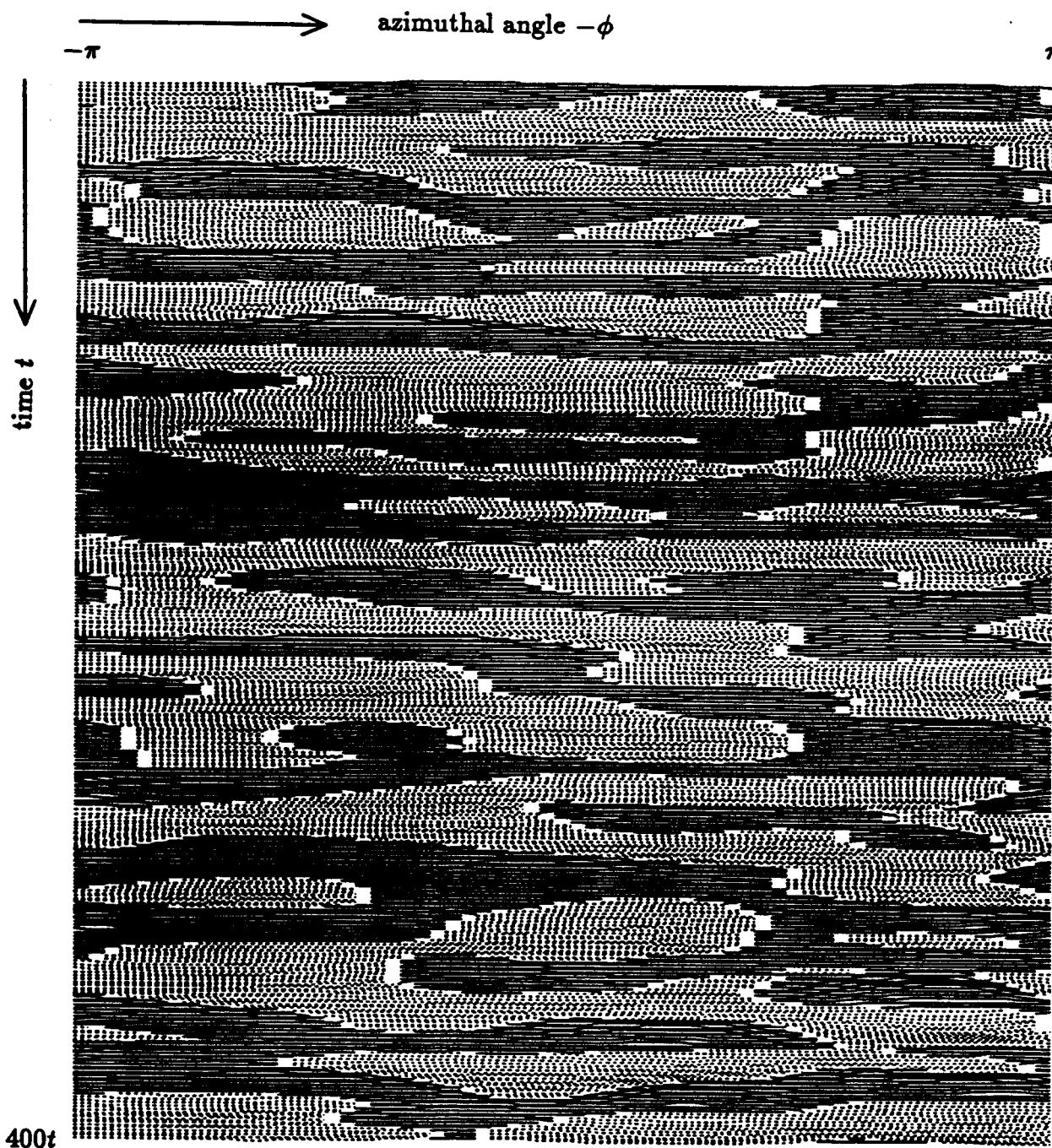
Figure 13: Azimuthal imprints of the vortical structures at $x/a = 5.76$. Signals were bandpass filtered with a $\frac{1}{3}$-octave FIR filter with $f_c = 70$ Hz. Impinging plate was installed.